ELectronics EXpress

LETTER IEICE Electronics Express, Vol.11, No.6, 1–10

Radar cross-section prediction based on shooting and bouncing rays using line tracing method

Hyun-Seok Lee[1a)], Hyun-Gyu Park[2], Hyo-Tae Kim[1], and Kyung-Tae Kim[1b)]

[1] *Department of Electrical Engineering, Postech, 77 Cheongam-ro, Nam-gu, Pohang, Gyeongbuk 790–784, Korea*

[2] *Agency for Defense Development (ADD), Sunam-dong, Yuseong-gu, Daejeon 305–152, Korea*

a) *lehyuni@postech.ac.kr*

b) *kkt@postech.ac.kr*

Abstract: High-frequency predictions of radar cross-sections are usually performed using the well-known shooting and bouncing rays (SBR) method. SBR needs many incident ray tubes for accurate results. Therefore, its computation time is proportional to the square of the number of ray tubes, often resulting in a prohibitively large computation time, especially for electrically large and complex objects. To address this problem, a new ray tube merging scheme called line tracing SBR (LT-SBR) is proposed to reduce the number of incident rays. Simulation results reveal that the LT-SBR has a computational advantage over the conventional SBR and recently introduced beam tracing SBR.

Keywords: RCS, prediction, SBR, line, tracing

Classification: Electromagnetic theory

References

[1] H. Ling, R. C. Chou and S. W. Lee: IEEE Trans. Antennas Propag. **37** [2] (1989) 194.

[2] D. Klement, J. Preissner and V. Stein: IEEE Trans. Antennas Propag. **36** [2] (1988) 228.

[3] S.-H. Suk, T.-I. Seo, H.-S. Park and H.-T. Kim: Microw. Opt. Tech. Lett. **29** [6] (2001) 394.

[4] H.-G. Park, H.-T. Kim and K.-T. Kim: Prog. Electromagnetics Res. M **20** (2011) 29.

DOI: 10.1587/elex.11.20140102
Received February 03, 2014
Accepted February 12, 2014
Publicized March 05, 2014
Copyedited March 25, 2014

1 Introduction

In the field of radar cross section (RCS) prediction of electrically large and complex targets, the shooting and bouncing rays (SBR) method [1] was developed to supplement physical optics (PO) [2], which takes into consideration the first-order reflections. Because SBR traces incident ray

IEICE Electronics Express, Vol.11, No.6, 1–10

tubes before surface integration based on PO, it can predict RCS of complex targets in cases with multiple scattering. However, predictions based on the conventional SBR need more time as the target's size increases. In general, many incident ray tubes are required in a dense grid ($<\lambda/10$) to obtain accuracy and the area generating incident ray tubes should be sufficiently sized for targets with large dimensions. Therefore, the computation time of SBR is proportional to the square of the number of incident ray tubes. There have been several trials to reduce the number of incident ray tubes to save computation time.

The multiresolution grid algorithm in SBR (M-SBR) was proposed to decrease the number of redundant ray tubes with adaptive ray grid generation [3]. When some ray tubes hit one of the target's facets, M-SBR merges several incident ray tubes into a single tube with a coarser grid. In this method, however, the resolution of ray tubes passing or impacting around the boundaries of facets cannot be changed. Thus, the computation time is still squarely proportional to the increase in a target's size. The beam-tracing SBR (BT-SBR) was recently developed to address this drawback [4]. BT-SBR models the incident plane wave as a set of trigonal ray tubes whose cross sections are directly shown partitions of the facets. Because each ray tube is traced and recursively subdivided as it reflects from the target, the computation time of BT-SBR is independent of the size of the target, and the number of ray tubes in the method can be greatly decreased especially for electrically large targets. However, the computation time of BT-SBR increases much more rapidly than that of M-SBR as the number of the target's facets increases, owing to the additional time required to reshape beam tubes for each facet of the target.

In this paper, we propose a line tracing SBR (LT-SBR) method that merges ray tubes in a linear fashion. In this method, some ray tubes of the conventional method are merged into a single one, called a line tube. In addition, intersection lines are calculated instead of intersection points. LT-SBR can calculate the RCS of the target much faster than the conventional SBR because its computation time is linearly proportional to the target's size. Furthermore, it has faster computation speed than BT-SBR as the number of target's facets increase because it does not need additional time for generating beam tubes.

Following this introduction, we discuss the LT-SBR procedure in Section 2. Section 3 presents RCS prediction of some models to verify the efficiency of the LT-SBR, followed by the conclusion in Section 4.

2 Line tracing method

In the conventional SBR, parallel ray tubes consisting of plane waves are generated in a uniform grid, as shown in Fig. 1-(a) [1]. To obtain a convergent result, the grid density should be greater than ten ray tubes per wavelength and the size of each ray tube should be less than $0.1\lambda \times 0.1\lambda$. The number of ray tubes is inversely proportional to the size of each ray tube. The center of each small ray tube is traced to find the hit point on the facet (shown as a dot in Fig. 1-(a)). On the other hand, several small ray tubes in SBR are merged to a single large one in the proposed LT-SBR. In particular, it makes use of the center line (shown as a thick line in Fig. 1-(b)) of each merged large ray tube along the specific direction (shown as $\hat{x}$

DOI: 10.1587/elex.11.20140102
Received February 03, 2014
Accepted February 12, 2014
Publicized March 05, 2014
Copyedited March 25, 2014

IEICE Electronics Express, Vol.11, No.6, 1–10

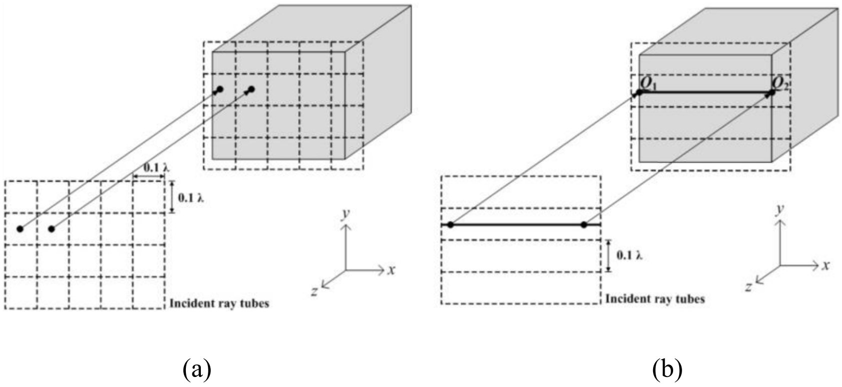

Fig. 1. (a) Ray tubes of the conventional SBR and (b) line tubes of LT-SBR.

-axis in Fig. 1-(b)) to find the hit point on the facet, instead of the center point as in the conventional SBR. The large merged ray tubes are called "line tubes.".

As shown in Fig. 1, incident ray tubes in SBR traveling toward the $-\hat{z}$ direction are merged along the horizontal direction, which produces line tubes along the $\hat{x}$ direction. Therefore, the number of line tubes is proportional to the electrical length of the target along the vertical direction ($\hat{y}$ direction). The line tracing is used to determine the intersection line $\overline{Q_1Q_2}$ on each facet of the target.

For the sake of computational convenience, the geometric model of the target is rotated such that the incident rays always travel toward the $-\hat{z}$ direction. If the incident line tube launching at y_i meets the trigonal facet having three vertices, P_1 (x_1, y_1, z_1), P_2 (x_2, y_2, z_2), and P_3 (x_3, y_3, z_3), the following relation holds:

$$\min(y_1, y_2, y_3) \leq y_i \leq \max(y_1, y_2, y_3) \tag{1}$$

Otherwise, there is no intersection line between the incident line tube and the facet. If the incident line tube hits on the facet as shown in Fig. 2, the intersection line $\overline{Q_1Q_2}$ will correspond to the intersection between the line tube and two edges $\overline{P_1P_2}$ and $\overline{P_2P_3}$ of the trigonal facet as follows:

$$Q_1 : \frac{x - x_1}{x_2 - x_1} = \frac{y - y_1}{y_2 - y_1} = \frac{z - z_1}{z_2 - z_1}$$
$$\begin{cases} y_{q1} = y_i \\ x_{q1} = \dfrac{(y_i - y_1)}{(y_2 - y_1)}(x_2 - x_1) + x_1 \\ \mathrm{z}_{q1} = \dfrac{(y_i - y_1)}{(y_2 - y_1)}(z_2 - z_1) + z_1 \end{cases} \tag{2-a}$$

$$Q_2 : \frac{x - x_3}{x_2 - x_3} = \frac{y - y_3}{y_2 - y_3} = \frac{z - z_3}{z_2 - z_3}$$
$$\begin{cases} y_{q2} = y_i \\ x_{q2} = \dfrac{(y_i - y_3)}{(y_2 - y_3)}(x_2 - x_3) + x_3 \\ \mathrm{z}_{q2} = \dfrac{(y_i - y_3)}{(y_2 - y_3)}(z_2 - z_3) + z_3 \end{cases} \tag{2-b}$$

DOI: 10.1587/elex.11.20140102
Received February 03, 2014
Accepted February 12, 2014
Publicized March 05, 2014
Copyedited March 25, 2014

IEICE Electronics Express, Vol.11, No.6, 1–10

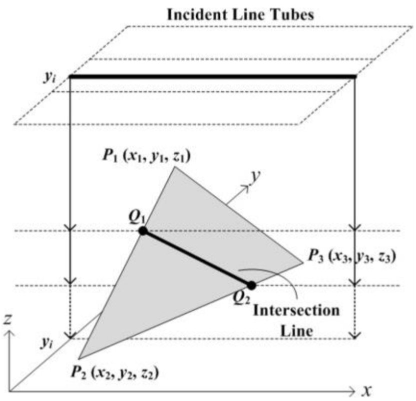

Fig. 2. An intersection line when the incident line tube travels toward the $-\hat{z}$ direction.

In second- or higher-order reflections, there are four different cases of intersection lines between the line tube and the two edge lines of the facet. Among them, the intersection lines of the first two cases (a) and (b) in Fig. 3 can be easily determined using eq. (2-a) and (2-b). In the cases (c) and (d), the intersection lines correspond to the incident line tube and the plane containing the facet, as shown in Fig. 4. In particular, the intersection points R_1 and R_2 between the two lines $\overline{Q_1R_1}$ and $\overline{Q_2R_2}$ of the incident line tube and plane with its normal vector $(a_f,\ b_f,\ c_f)$ form the desired intersection line $\overline{R_1R_2}$. The two lines $\overline{Q_1R_1}$ and $\overline{Q_2R_2}$ whose direction vector is $(a_i,\ b_i,\ c_i)$ are respectively given by

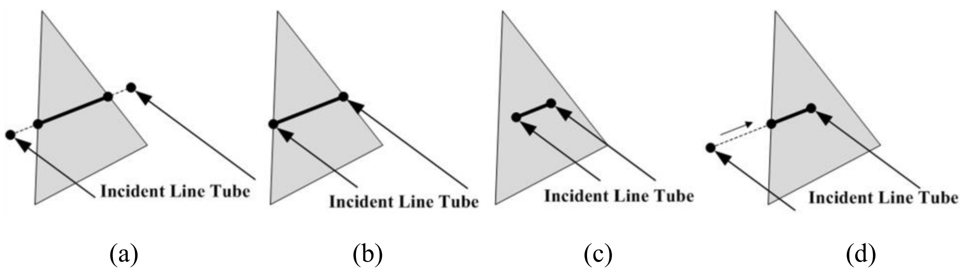

Fig. 3. The intersection lines of second- or higher-order reflection.

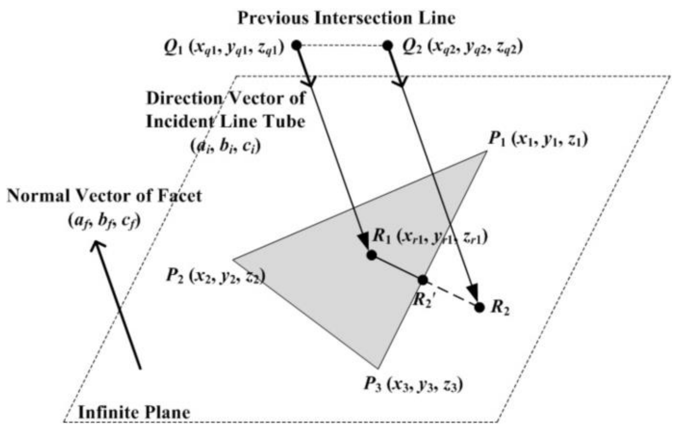

Fig. 4. The end points of an intersection line in second- or higher-order reflections.

DOI: 10.1587/elex.11.20140102
Received February 03, 2014
Accepted February 12, 2014
Publicized March 05, 2014
Copyedited March 25, 2014

IEICE Electronics Express, Vol.11, No.6, 1–10

$$\frac{x - x_{q1}}{a_i} = \frac{y - y_{q1}}{b_i} = \frac{z - z_{q1}}{c_i} \tag{3-a}$$

$$\frac{x - x_{q2}}{a_i} = \frac{y - y_{q2}}{b_i} = \frac{z - z_{q2}}{c_i} \tag{3-b}$$

In addition, the plane containing the facet whose normal vector (a_f, b_f, c_f) and known vertex of the facet P_1 (x_1, y_1, z_1) yields

$$a_f(x - x_1) + b_f(y - y_1) + c_f(z - z_1) = 0 \tag{4}$$

Therefore, the intersection point R_1 can be obtained by the intersection between the line in Eq. (3-a) and the plane in Eq. (4). The results are as follows:

$$\begin{cases} x_{r1} = \dfrac{a_f a_i x_1 + (b_f b_i + c_f c_i)x_{q1} - b_f a_i (y_{q1} - y_1) - c_f a_i (z_{q1} - z_1)}{a_f a_i + b_f b_i + c_f c_i} \\ y_{r1} = \dfrac{b_i}{a_i}(x_{r1} - x_{q1}) + y_{q1} \\ z_{r1} = \dfrac{c_i}{a_i}(x_{r1} - x_{q1}) + z_{q1} \end{cases} \quad \text{when } a_i \neq 0 \tag{5-a}$$

$$\begin{cases} x_{r1} = x_{q1} \\ y_{r1} = -\dfrac{a_f b_i (x_{q1} - x_1) - b_f b_i y_1 - c_f c_i y_{q1} + c_f b_i (z_{q1} - z_1)}{b_f b_i + c_f c_i} \\ z_{r1} = \dfrac{c_i}{b_i}(y_{r1} - y_{q1}) + z_{q1} \end{cases} \quad \text{when } a_i = 0 \text{ and } b_i \neq 0 \tag{5-b}$$

$$\begin{cases} x_{r1} = x_{q1} \\ y_{r1} = y_{q1} \\ z_{r1} = -\dfrac{a_f(x_{q1} - x_1) + b_f(y_{q1} - y_1)}{c_f} + z_1 \end{cases} \quad \text{when } a_i = b_i = 0 \tag{5-c}$$

It should be noted that the general solution in (5-a) should be modified to (5-b) or (5-c), when $a_i = 0$ and $b_i \neq 0$, or $a_i = b_i = 0$ respectively. R_2 can be determined in the same manner in (5-a), (5-b) and (5-c) if R_2 is within the facet (i.e., Fig. 3-(c)). However, if R_2 is outside the facet (i.e., Fig. 3-(d)), an additional computation is required to find the intersection point R_2' between the line $\overline{R_1R_2}$ and the edge line $\overline{P_1P_3}$.

The intersection lines can be overlapped partially or entirely, because intersection lines are individually calculated for all facets and some facets can be shadowed by other facets. In the cases shown in Fig. 5-(a) and (b), the overlapped part of each intersection line described as a dotted line (lower parts of (a) and (b)) should be removed. This removal process is similar to "the hidden facet removal" of the conventional SBR [1]. Furthermore, if two facets share the same plane and the side edge as shown in Fig 5-(c), the two separate intersection lines can be joined to form a single one. This joining process can be extended to numerous facets greater than two, and therefore it is an essential step for reducing computational complexity.

If a single line tube hits two or more facets whose normal vectors are

DOI: 10.1587/elex.11.20140102
Received February 03, 2014
Accepted February 12, 2014
Publicized March 05, 2014
Copyedited March 25, 2014

IEICE Electronics Express, Vol.11, No.6, 1–10

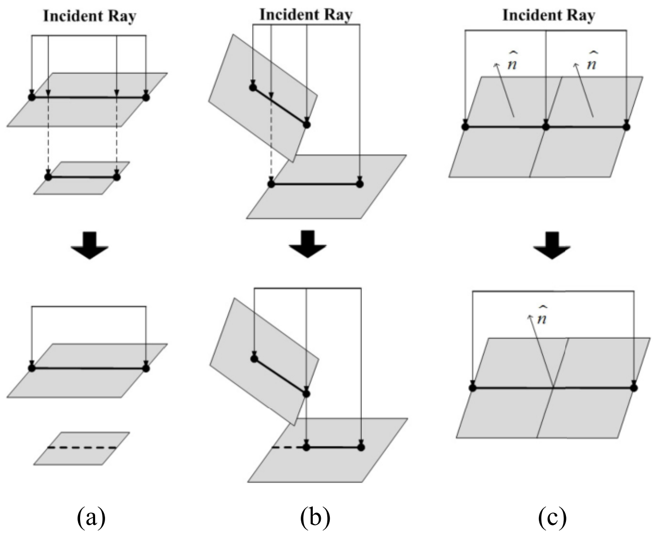

Fig. 5. (a), (b) The removal process and (c) the joining process.

different, then the single line tube should be divided to calculate each path length as shown in Fig. 6-(a). We can construct virtual facets using the stored path length for each ray as shown in Fig. 6-(b), and thus, the final scattered fields can be calculated by the panel evaluations of PO integrations [2].

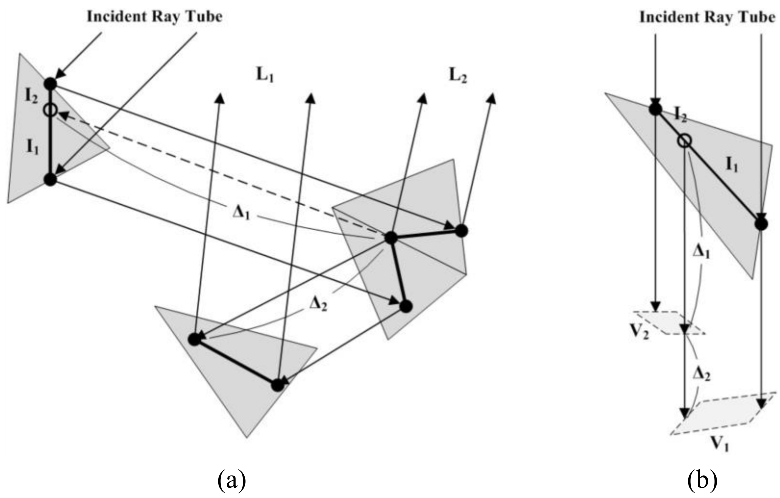

Fig. 6. (a) Intersection line division. (b) Virtual facets.

The overall algorithm of LT-SBR so far is summarized as follows.

3 Simulation results

The simple ship model made of perfect electric conductor (PEC) in Fig. 8 is used to verify the proposed LT-SBR in terms of RCS prediction, which is carried out along both the azimuth and elevation plane as shown in Fig. 9.

In Fig. 9, the results of method of moments (MoM) obtained from commercial software FEKO and those of the conventional SBR are also presented for the purpose of comparison. It is worth to note that the results of the LT-SBR and SBR show a good agreement with that of the MoM.

DOI: 10.1587/elex.11.20140102
Received February 03, 2014
Accepted February 12, 2014
Publicized March 05, 2014
Copyedited March 25, 2014

IEICE Electronics Express, Vol.11, No.6, 1–10

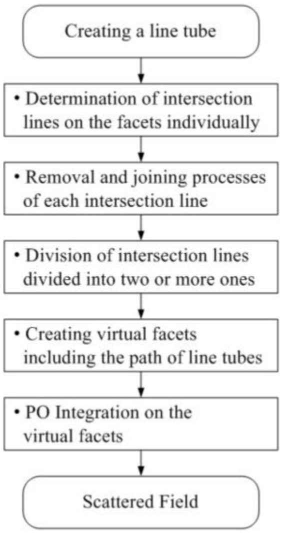

Fig. 7. Block diagram of overall algorithm.

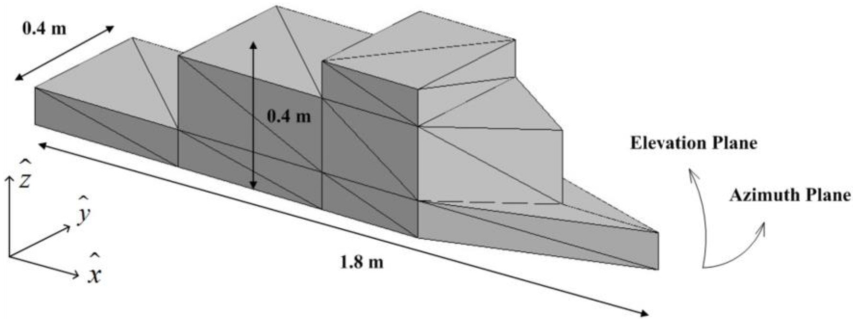

Fig. 8. Geometry of the simple ship model (56 facets).

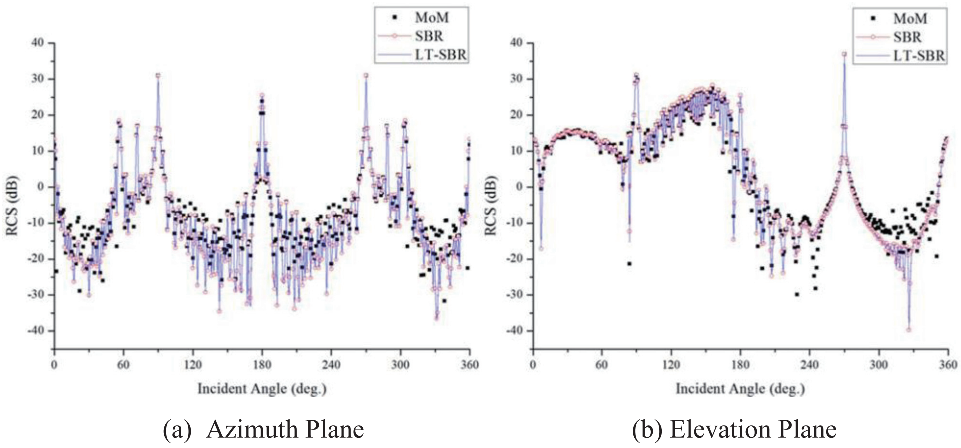

Fig. 9. Monostatic RCS prediction of the simple ship model.

This implies that the proposed LT-SBR has a reasonable accuracy in terms of RCS prediction.

To investigate the computational efficiency of LT-SBR, the size of the ship model in Fig. 8 is varied from 5 to 20 times of the original size. However, note that the number of facets modeling the ship model remains fixed at 56 even though its size increases. In conventional SBR, it is well known that the number of incident rays dramatically increases as the target size becomes large, resulting in high computational complexity.

DOI: 10.1587/elex.11.20140102
Received February 03, 2014
Accepted February 12, 2014
Publicized March 05, 2014
Copyedited March 25, 2014

IEICE Electronics Express, Vol.11, No.6, 1–10

Fig. 10 shows the effects of target scale (i.e., number of incident ray tubes) on the computation time of the both SBR and LT-SBR. As expected, the increase in the computation time of SBR against target size is proportional to the square of the target size, whereas that of LT-SBR is linearly proportional to the target size, which yields a significant computational benefit. This is because the LT-SBR merges many incident ray tubes into a single one, effectively decreasing the number of incident rays.

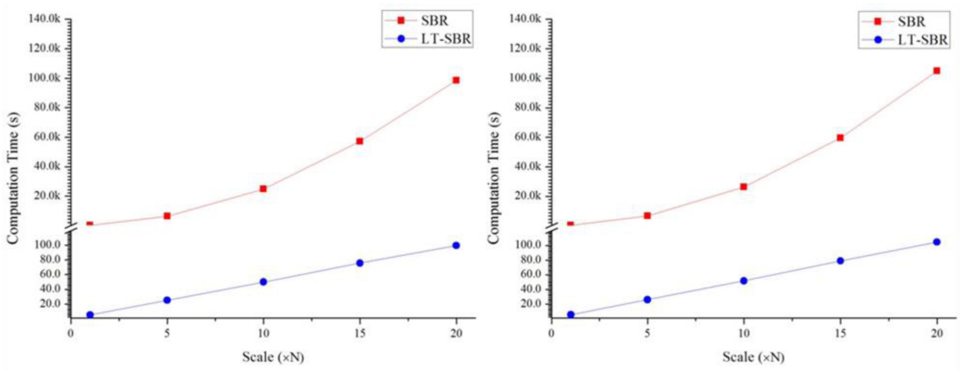

(a) Azimuth Plane (b) Elevation Plane

Fig. 10. Computation time of the simple ship models in various scales.

However, this benefit due to merging incident rays depends on the target geometry. For the ship model in Fig. 8, the target's horizontal dimension is much larger than the vertical dimension from the side of the target. In this case, the number of line tubes for the $\hat{x}$ (horizontal) direction is much smaller than that of the $\hat{y}$ (vertical) direction, as shown in Fig. 11. The $\hat{x}$-directed line tubes can give much more computational advantages than $\hat{y}$-directed line tubes, as shown in Fig. 12. As a result, to accelerate the computational speed of LT-SBR, it is recommended that the direction of incident line tubes coincides with that of the longer dimension of the target for each specific direction.

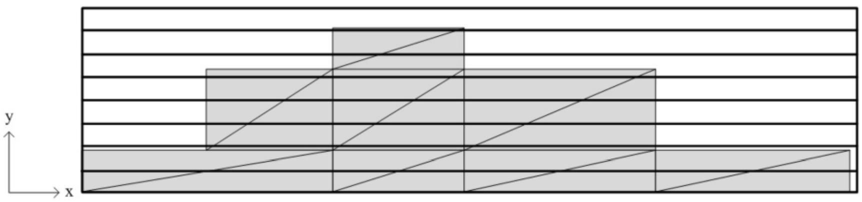

(a)

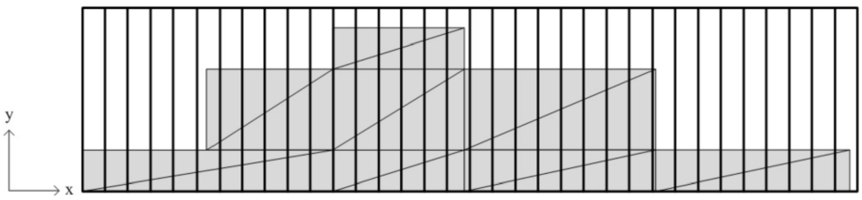

(b)

Fig. 11. The line tubes of different directions.

The RCS of the helicopter model in Fig. 13 was calculated as the number of facets varied with the target's size remaining fixed. Fig. 14 shows RCS prediction results of the helicopter model consisting of 9836

DOI: 10.1587/elex.11.20140102
Received February 03, 2014
Accepted February 12, 2014
Publicized March 05, 2014
Copyedited March 25, 2014

IEICE Electronics Express, Vol.11, No.6, 1–10

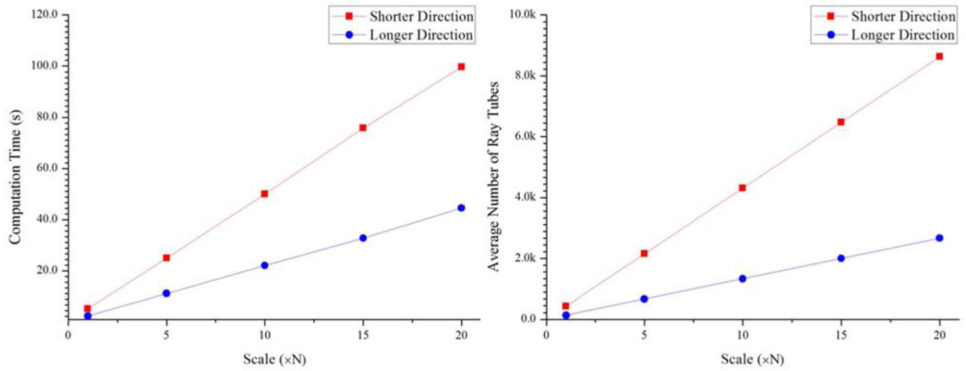

(a) Azimuth Plane (b) Elevation Plane

Fig. 12. Computation time of simple ship models along different directions.

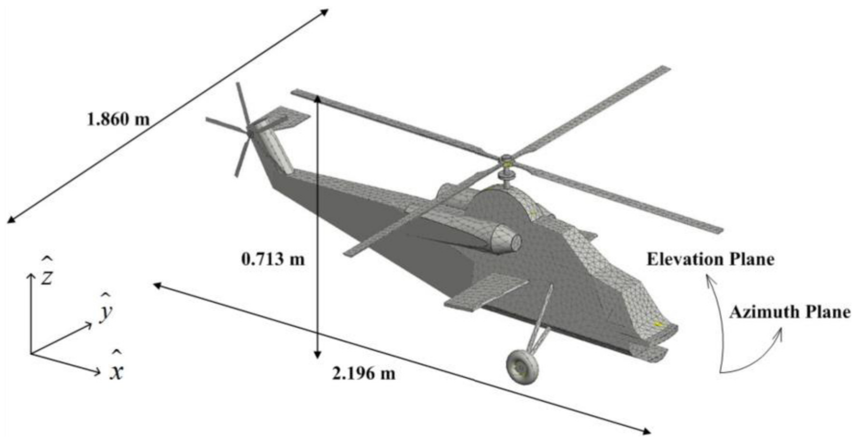

Fig. 13. Geometry of the helicopter model (9836 facets).

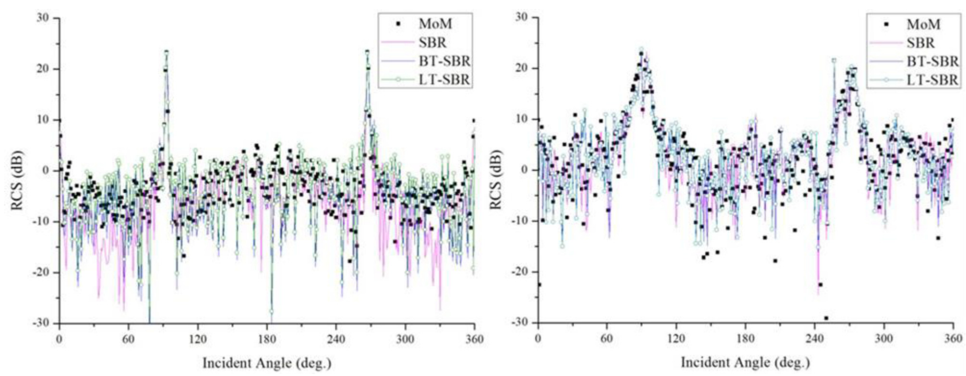

(a) Azimuth Plane (b) Elevation Plane

Fig. 14. Monostatic RCS prediction of the helicopter model.

facets. It is quite apparent from Fig. 14 that the proposed LT-SBR predicts RCS with an accuracy level comparable with MoM, conventional SBR, and BT-SBR.

The computational efficiency of the LT-SBR is illustrated in Fig. 15 as the number of facets increases when the target's dimension remains unchanged, which is the opposite case to the results in Fig. 10. The computational efficiency of BT-SBR and LT-SBR is substantially superior to that of conventional SBR. In addition, the benefit of LT-SBR becomes

DOI: 10.1587/elex.11.20140102
Received February 03, 2014
Accepted February 12, 2014
Publicized March 05, 2014
Copyedited March 25, 2014

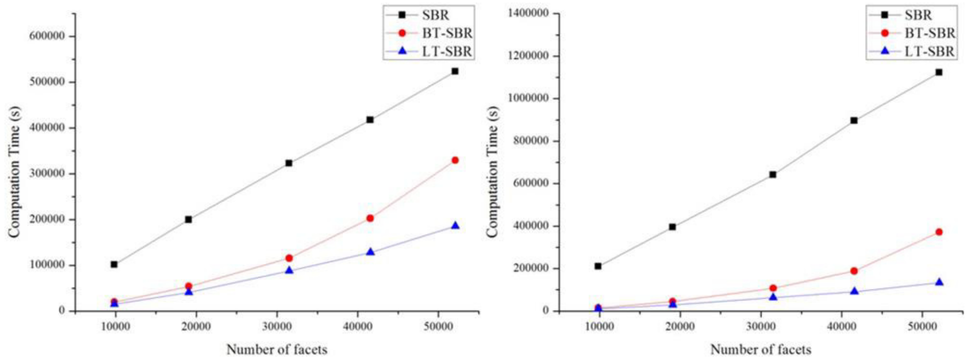

(a) Azimuth Plane (b) Elevation Plane

Fig. 15. Computation time of helicopter models in the various numbers of facets.

much more pronounced as the number of facets increases, providing better computational efficiency than BT-SBR.

4 Conclusion

This paper proposed the LT-SBR method based on a new ray tube merging scheme. Some small ray tubes in the conventional SBR are merged to a large single one in the proposed method, and thus it improves computation speed in the prediction of an electrically large target's RCS. Furthermore, when the target's structural complexity increases due to the number of facets, LT-SBR is a more efficient calculation method. The accuracy of LT-SBR was verified in comparison with MoM, and the results were similar to other SBR methods.

It should be noted that the computation of BT-SBR is independent of the target's size, but it is proportional to the number of facets [4]. Therefore, BT-SBR is more appropriate for large and geometrically simple targets such as buildings in an urban environment. In contrast, the computation time of LT-SBR depends not only on the target's dimension but also on the number of facets modeling the target. However, its computation time is much lower than that of BT-SBR especially for a large number of facets, which often occurs for geometrically complex targets, like helicopters, tanks, and battle ships.

DOI: 10.1587/elex.11.20140102
Received February 03, 2014
Accepted February 12, 2014
Publicized March 05, 2014
Copyedited March 25, 2014